NUMERICAL AND EXPERIMENTAL INVESTIGATION OF A DOUBLE-PIPE HEAT EXCHANGER WITH SiO_2 NANO-ADDITIVES

Fatih Selimefendigil,[1] Ceylin Şirin,[1,] & Hakan F. Öztop[2]*

[1]*Department of Mechanical Engineering, Manisa Celal Bayar University, 45140 Manisa, Turkey*

[2]*Department of Mechanical Engineering, Technology Faculty, Fırat University, 23119 Elazığ, Turkey*

*Address all correspondence to: Ceylin Şirin, Department of Mechanical Engineering, Manisa Celal Bayar University, 45140 Manisa, Turkey; Tel.: +902362412144; Fax: +902362012020, E-mail: cceylinsirinn@gmail.com

Original Manuscript Submitted: 4/20/2021; Final Draft Received: 9/23/2021

In this work, numerical and experimental analyses of a double-pipe heat exchanger with SiO_2 nanoparticles were performed. The numerical study was conducted by using the k–ε turbulence model with the Galerkin weighted residual finite element method. The nanofluid was used in the inner pipe at various solid particle volume fractions. Effects of flow rate and temperature on the overall heat transfer coefficient were examined. The Brownian motion effect was included in the effective thermal conductivity of the nanofluid. It was observed that the overall heat transfer coefficient enhanced with the inclusion of nanoparticle and increasing the volumetric flow rate of nanofluid. Even though the validation of the experimental study was conducted, there are discrepancies between the numerical and experimental studies which become higher for a higher mass flow rate. The deviations are 4.60% and 27.50% at volumetric flow rates of 0.87 L/min and 2.15 L/min.

KEY WORDS: *nanofluid, SiO_2, heat exchanger, finite element method, 3D turbulent*

1. INTRODUCTION

Energy demands are increasing day by day with developing industrialization and population (Sözen et al., 2020; Khanlari et al., 2020). Due to the limitation of fossil energy resources, research and applications related to effective utilization of both electrical and thermal energy have increased worldwide (Tuncer et al., 2021).

One of the effective methods for upgrading the performance of thermal systems is utilization of nanofluids as a working fluid. Use of nanofluids in thermal engineering systems captures great attention nowadays. Metallic or nonmetallic additives to the base fluid enhance the thermal conductivity of the base fluid (Khanlari, 2020; Selimefendigil and Öztop, 2019). The conductivity of heat transfer fluids such as water or ethylene glycol is very low when compared to metallic nanoparticles. When nanoparticles are added to the base fluid in very low amount, thermal conductivity increases significantly. Thus, it is possible to obtain compact, low-weight thermal engineering systems. The environmental side effects can be reduced as a result of low energy consumption. There are many applications for nanofluids in thermal engineering field ranging from solar power to refrigeration (Gürbüz et al., 2020; Selimefendigil and Oztop, 2017; Chen et al., 2017; Ho et al., 2020; Aidaoui et al., 2020). In a study conducted by Saffarian et al. (2020), solar collectors with various flow channels were analyzed. CuO and Al_2O_3-based nanofluids were utilized in the solar heating system. The findings obtained showed that using wavy pipe design and CuO-based nanofluid increased the heat transfer by approximately 78%. Moravej et al. (2020) utilized rutile TiO_2/water nanofluids to increase the thermal performance of a symmetrical flat-plate solar collector. They used three different concentrations in the investigation (1, 3, and 5 wt.%). In another work, Selimefendigil and Öztop (2021) studied the enhancement of thermoelectric device performance by using nanofluids and rotating cylinders in a channel flow to be utilized in renewable energy systems.

1064-2285/22/$35.00

NOMENCLATURE

h	local heat transfer coefficient	**Greek Symbols**	
k	thermal conductivity	α	thermal diffusivity
L	pipe length	θ	nondimensional temperature
n	unit normal vector	ν	kinematic viscosity
Nu_x	local Nusselt number	ρ	density of the fluid
Nu_m	average Nusselt number	ϕ	solid volume fraction
p	pressure	**Subscripts**	
Pr	Prandtl number	c	cold
T	temperature	h	hot
u, v, w	x, y, z velocity components	m	average
		nf	nanofluid
x, y, z	Cartesian coordinates	w	wall

Double-pipe heat exchangers generally were used for heating and cooling of process fluids where small heat transfer areas are required. They can be assembled in series to increase the thermal capacity and heat transfer surface area and they can withstand high pressures. There are some studies about utilizing nanofluids in double-pipe heat exchangers available in the literature. Also, Shirvan et al. (2017) numerically analyzed the effect of utilizing Al_2O_3/water nanofluid in double-pipe heat exchangers. They also modeled findings by using statistical approaches. Demir et al. (2011) performed numerical analysis for the hydrothermal behavior of a double-pipe heat exchanger containing nanofluids. They used water and TiO_2 and Al_2O_3 nanoparticles. It was shown that the increase in heat transfer is much greater than the increase in pressure loss. In another study, Mahbubul et al. (2013) investigated the heat transfer and pressure loss in a horizontal smooth pipe by using nanorefrigerants containing alumina nanoparticles. They used various solid nanoparticle volume fractions between 1% and 5%. They showed that an optimum solid particle volume fraction is achieved to obtain the best performance in a cooling system. Chun et al. (2009) examined the laminar heat transfer in a double-pipe heat exchanger with nanofluids. From the experimental study they showed that the surface properties of nanoparticles are the main factors in the enhancement of the heat transfer. They obtained higher heat transfer coefficient as the solid particle volume fraction increases. In many studies, it is shown that a compact lightweight heat exchanger can be obtained when nanoparticles are added to the base fluid. The heat transfer performance depends on many factors such as nanoparticle type, nanoparticle shape, and solid volume fraction of the nanoparticles. The thermal conductivity enhancement of the base fluid when nanoparticles are added depends on some of these factors. In the application, many metallic or nonmetallic nanoparticles are used which have spherical shape and have average particle diameter between 10 nm and 50 nm. In a recent review study, application of the nanofluids in various types of heat exchangers is reported (Bahiraei et al., 2018).

In this study, numerical and experimental analyses for the thermal performance improvement of a double-pipe heat exchanger with SiO_2 nanoparticles inclusion to the water were performed. Various solid nanoparticle volume fractions were tested for different mass flow rates and temperatures and findigs were discussed in detail.

2. NUMERICAL MODELING

A schematic description of numerical model of the double-pipe heat exchanger is presented in Fig. 1. The inner and outer radii of the pipes are R_1 and R_2, while d_s and d_{ext} denote the interface and outer pipe thicknesses. Nanofluids with water as base fluid and SiO_2 as nanoparticles at various solid particle volume fractions were used. Table 1 lists

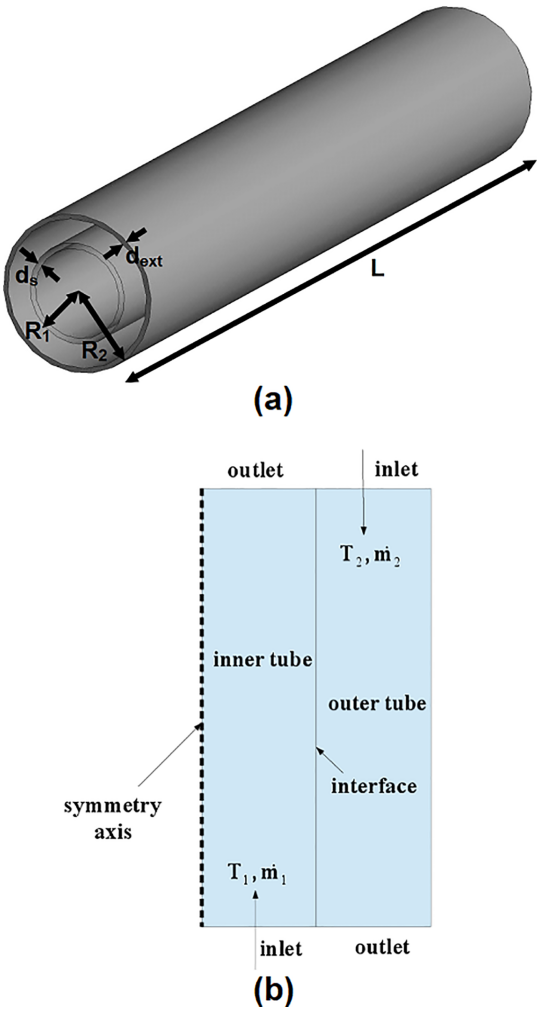

FIG. 1: Schematic description of double-pipe heat exchanger model in 3D (a) and 2D view with boundary conditions (b)

TABLE 1: Thermophysical properties of base fluid and SiO_2 nanoparticle [adapted from Vanaki et al. (2014)]

Property	Water	SiO_2
ρ (kg/m^3)	998.2	2200
c_p (J/kg K)	4812	703
k (W/m K)	0.61	1.2
μ (N s/m^2)	0.001003	—

the thermophysical properties of the base fluid and nanoparticles. The nanofluid with entrance temperature T_1 and mass flow rate $\dot{m}_1$ flows in the inner pipe, while the water flow in the annulus section has the entrance temperature T_2 and mass flow rate $\dot{m}_2$. Tables 2 and 3 present the geometrical and operating conditions of the numerical model. The values of T_2 and $\dot{m}_2$ are fixed to the values shown in the table while the values of T_1 and $\dot{m}_1$ varied during numerical study.

TABLE 2: Geometrical properties of double-pipe heat exchanger

Symbol	Value	Description
R_1	0.007 m	inner radius
R_2	0.015 m	outer radius
L	0.5 m	length
d_s	0.001 m	interface thickness
d_{ext}	0.005 m	outer pipe thickness
vol	3.5343×10^{-4} m^3	overall volume
beta	62.222 1/m	compactness

TABLE 3: System operating parameters

Symbol	Value	Description
T_1	314.6 K	inner pipe inlet temperature
T_2	292.8 K	annulus inlet temperature
$\dot{m}_1$	0.0145 kg/s	inner pipe mass flow rate
$\dot{m}_2$	0.0395 kg/s	annulus mass flow rate
pA1	101.3 kPa	inner pipe exit pressure
pA2	101.3 kPa	annulus exit pressure

The fluid was assumed to be Newtonian and incompressible. The flow is three-dimensional, steady, and turbulent. Effects of viscous dissipation, radiation, and natural convection were all neglected.

Three-dimensional steady flow equations with the k–ε turbulence model were used and they can be stated as follows:

$$\frac{\partial(u_i)}{\partial x_i} = 0 \tag{1}$$

$$\frac{\partial(\rho_{nf} u_i u_j)}{\partial x_j} = -\frac{\partial p}{\partial x_i} + \frac{\partial(-\rho_{nf} u_i' u_j')}{\partial x_i} + \frac{\partial\left(\mu_{nf}\left(\frac{\partial u_i}{\partial x_j} + \frac{\partial u_j}{\partial x_i}\right)\right)}{\partial x_j} \tag{2}$$

$$\frac{\partial(\rho_{nf} u_i T)}{\partial x_i} = \frac{\partial\left((\Gamma + \Gamma_t)\frac{\partial T}{\partial x_i}\right)}{\partial x_i} \tag{3}$$

$$\frac{\partial(\rho_{nf} u_i k)}{\partial x_i} = \frac{\partial\left(\left(\frac{\mu_t}{\sigma_k} + \mu_{nf}\right)\frac{\partial k}{\partial x_j}\right)}{\partial x_j} - \rho_{nf}\epsilon + G_k \tag{4}$$

$$\frac{\partial(\rho_{nf} u_i \epsilon)}{\partial x_i} = \frac{\partial\left(\left(\frac{\mu_t}{\sigma_k} + \mu_{nf}\right)\frac{\partial \epsilon}{\partial x_j}\right)}{\partial x_j} + \frac{\epsilon}{k} G_k C_{1\epsilon} - \rho_{nf} \frac{\epsilon^2}{k} C_{2\epsilon} \tag{5}$$

with

$$-\rho_{nf} u_i' u_j' = \mu_t \left(\frac{\partial u_i}{\partial x_j} + \frac{\partial u_j}{\partial x_i}\right) - \frac{2}{3}\rho_{nf} k \delta_{ij} - \frac{2}{3}\rho_{nf} \mu_t \frac{\partial u_k}{\partial u_j} \delta_{ij}$$

$$\mu_t = \frac{\rho_{nf} C_\mu k^2 \epsilon}{,} G_k = -\frac{\partial u_j}{\partial x_i} \rho_{nf} u_i' u_j' \tag{6}$$

$C_{1\epsilon} = 1.42$, $C_\mu = 0.0845$, $C_{2\epsilon} = 1.68$, $Pr_t = 0.85$, $\sigma_k = 1$, $\sigma_\epsilon = 1.3$

It also considered the conduction in the interface between the fluids in the inner pipe and in the annulus part as

$$\frac{\partial^2 T}{\partial x^2} + \frac{\partial^2 T}{\partial y^2} + \frac{\partial^2 T}{\partial z^2} = 0 \tag{7}$$

Constant hot and cold temperatures are assumed at the inlet of the inner pipe and annulus section as T_1 and T_2, while no-slip boundary conditions ($u = v = w = 0$) are imposed for the tube walls. Constant mass flow rates $\dot{m}_1$ and $\dot{m}_2$ are used at the inner and outer tube inlets. Pressure outlet boundary conditions are used at the exit of the inner pipe and annulus section. At the interfaces between conducting solid wall and inner pipe and annulus heat flux continuity was considered as

$$-k_c \left(\frac{\partial T}{\partial n}\right)_{c,i} = -k_h \left(\frac{\partial T}{\partial n}\right)_{h,i}$$

SiO_2 nanopatricles were used as additive to the water in the inner pipe. The effective density and specific heat of the nanofluid are given in terms of the base fluid, nanoparticle properties, and solid volume fraction as

$$\rho_{nf} + (1 - \phi)\, \rho_f + \phi \rho_p \tag{8}$$

$$(\rho c_p)_{nf} = (1 - \phi)(\rho c_p)_f + \phi (\rho c_p)_p \tag{9}$$

The effective thermal conductivity of the nanofluid includes the effect of Brownian motion and it can be given as (Vajjha et al., 2010)

$$k_{nf} = k_{sr} + k_{Brownian} \tag{10}$$

where k_{st} is defined by Maxwell (1904) as

$$k_{st} = k_f \left[\frac{(k_p + 2k_f) - 2\phi\,(k_f - k_p)}{(k_p + 2k_f) + \phi\,(k_f - k_p)} \right] \tag{11}$$

and $k_{Brownian}$ can be expressed by using the following equation:

$$k_{Brownian} = 5 \times 10^4 \times 1.9526 \times (100\phi)^{-1.4594} \phi \rho_f c_{p,f} \sqrt{\frac{k_b T}{\rho_p d_p}} f'(T,\phi) \tag{12}$$

where the function f' is given by Vajjha et al. (2010).

The effective viscosity model of the nanofluid can be found as (Corcione, 2010)

$$\mu_{nf} = \mu_f \frac{1}{\left(1 - 34.87\left(\frac{d_p}{d_f}\right)^{-0.3} \phi^{1.03}\right)} \tag{13}$$

with the average particle size of the fluid

$$d_f = \left(\frac{6M}{N\pi\rho_f}\right)^{\frac{1}{3}} \tag{14}$$

where M and N are the molecular weight and the Avogadro number, respectively.

The Galerkin weighted residual finite element method was used for the solution of governing equations with the appropriate boundary conditions as described above. In this method, weak form of the governing equations is established and residual R resulted when the approximated flow variables are inserted in the governing equations. A weighted average of this residual R will be forced to be zero:

$$\int_\Omega W_r R\, dv = 0 \tag{15}$$

where W_r represents the weight function which is chosen from the same set of functions as of the trial functions. At the nodes of internal element domain nonlinear residual equations are obtained and they are solved with Newton–Raphson method. Convergence of the solution is assured when the relative error for each of the flow variables satisfy convergence criteria which is less than 10^{-5}. Grid independence test of the numerical solution is verified by using different

number of grids. Following formulations are used to calculate the overall heat transfer coefficient of the double-pipe heat exchanger and to find its capacity or sizing of it:

overall heat transfer coefficient

$$\frac{1}{UA} = \sum R = \frac{1}{h_i A_i} + \frac{\ln(r_i r_o)}{2\pi kL} + \frac{1}{h_o A_o} \tag{16}$$

logarithmic mean temperature difference

$$\Delta T_{lm} = \frac{\Delta T_1 - \Delta T_2}{\ln\left(\frac{\Delta T_1}{\Delta T_2}\right)} \tag{17}$$

total heat transfer rate

$$\dot{Q} = (\dot{m} c_p (T_{in} - T_{out}))_c = (\dot{m} c_p (T_{in} - T_{out}))_{h'} \tag{18}$$

$$\dot{Q} = UA\Delta T_{lm} \tag{19}$$

where A is the total heat transfer surface area and $\dot{m}$ is the mass flow rate.

3. NUMERICAL STUDY

A numerical study for three-dimensional double-pipe heat exchanger with SiO_2 nanoparticles included in the hot water which circulates in the inner pipe is conducted. The geometrical and operating parameters are given in Tables 2 and 3. The annulus side volumetric flow rate is fixed to 2.36 L/min, while the inner pipe fluid flow rate and inlet temperature change which includes the nanofluid with various values of solid particle volume fraction. Figure 2 shows the variation of temperature in the annulus side for cold flow stream with various volumetric flow rates. As the mass flow of hot fluid rises, the exit temperature of the cold stream increases for fixed inlet temperature of the annulus. Including nanosized particles to the hot fluid results in heat transfer enhancement in the inner pipe and the overall heat coefficient increases. Figure 3 shows the variation of the overall heat transfer coefficient versus solid particle volume fraction for various flow rates $\dot{m}_1$ = 0.87 L/min, $\dot{m}_2$ = 2.15 L/min, and $\dot{m}_3$ = 2.37 L/min. The overall heat transfer coefficient increases when the values of flow rate and solid particle volume fraction augment. For nanofluid at the highest particle volume fraction, its value increases by about 16% for all flow rates $\dot{m}_1$, $\dot{m}_2$, and $\dot{m}_3$.

Effects of hot SiO_2–water nanofluid temperature on the overall heat transfer coefficient is shown in Fig. 4 for volumetric flow rate of 2.15 L/min considering various φ values. The U values at a temperature of T = 50°C is slightly higher than those at T = 40°C for all solid particle volume fractions (1.6% higher for water and 1.4% higher for nanofluid with φ = 2.5%).

4. EXPERIMENTAL STUDY

A double-pipe heat exchanger was used which is shown in Fig. 5. The measurement system consists of 2 turbine type flowmeters (accuracy, 3%), 4 temperature sensors (accuracy, 0.5°C). The setup is composed of control panel,

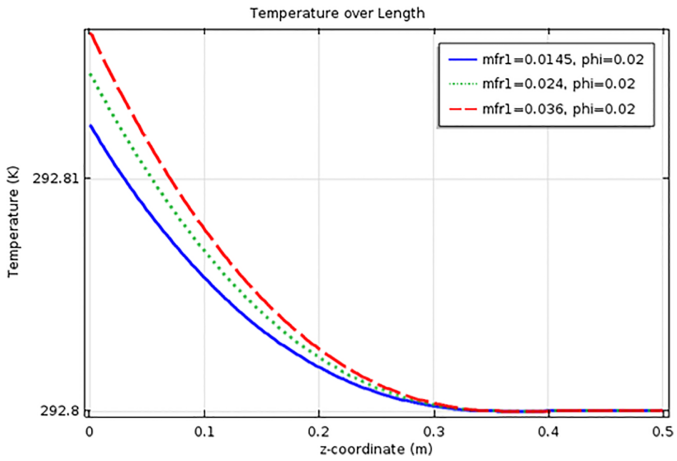

FIG. 2: Variation of temperature difference in the outlet for cold stream

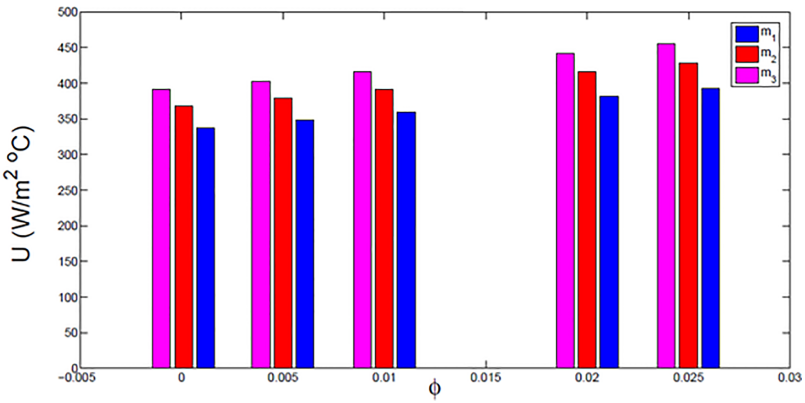

FIG. 3: Overall heat transfer coefficient versus solid particle volume fraction for different mass flow rates

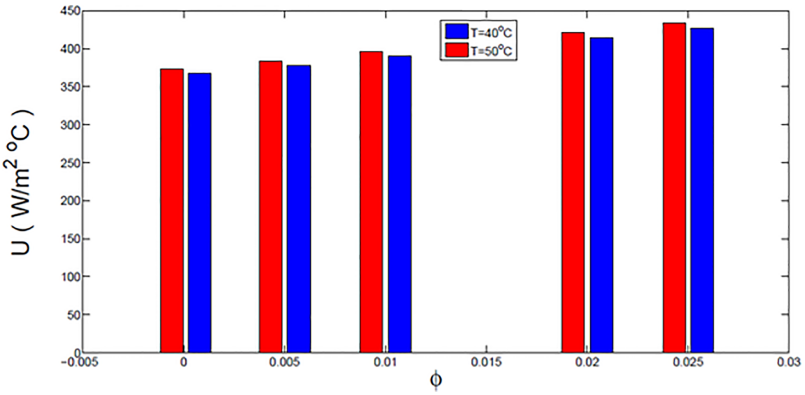

FIG. 4: Overall heat transfer coefficient versus solid particle volume fraction for different inlet temperatures

(a) (b)

FIG. 5: Experimental setup of double-pipe heat exchanger (a), water–SiO_2 nanofluid at various solid volume fractions (b)

hot and cold water feed units and heat exchanger. The flow rates and temperatures can be read from the control panel. The hot water is obtained by using a resistance type heater which is 2.5 kW. The water tank has a capacity of 15 L and is made of stainless steel. The inner pipe has an inner diameter of 14 mm and outer diameter of 16 mm. The length of the pipe is 500 mm. The outer pipe (the annulus side) has inner and outer diameters of 20 mm and 30 mm. The thermal conductivity of inner pipe is 16 W/m K. The hot water is flowing through the inner pipe while the cold water is circulated through the annulus side of the heat exchanger. The hot water temperature of the inner pipe is controlled by using the resistance heater and the flow rates area is also controlled. The SiO_2 nanoparticles are included in the hot water.

Different correlations can be used to find the heat transfer coefficient for the inner pipe and for the annulus side of the double-pipe heat exchanger and one of them can be stated as (Kakaç et al., 2020)

$$Nu = \frac{\left(\frac{f}{2}\right) RePr}{1 + 8.7\left(\frac{f}{2}\right)^{\frac{1}{2}} (Pr - 1)}, f = [1.58 \ln (Re - 3.28)]^{-2} \tag{20}$$

For the laminar flow configuration, the Sieder–Tate correlation can be used which has the following form (Kakaç et al., 2020):

$$Nu = 1.86\left(RePr \frac{D_h}{L} \right)^{\frac{1}{3}} \left(\frac{\mu_b}{\mu_w} \right)^{0.14} \tag{21}$$

In order the validate the experimental study, the size of the heat exchanger was determined by using the values from the control panel for the inner and outer flow rates and temperature of the inner pipe and annulus. By using the above-given correlations for the calculation of heat transfer coefficient and overall heat transfer coefficient as described in Eq. (16), the length of heat exchanger was found to be 517 mm and the actual length is 500 mm.

Figure 6 shows the variation of overall heat transfer coefficient versus solid particle volume fraction for two volumetric flow rates of the hot water flowing through the inner pipe. The flow rate of cold water in the annulus is fixed at 2.36 L/min. It is observed that the overall heat transfer coefficient enhances with solid particle volume fraction for all flow rates. Its value is also increasing for higher values of flow rates. Adding nanoparticles results in enhancement of the overall heat transfer coefficient and this is significant for higher values of flow rate. For flow rate 0.87 L/min, the

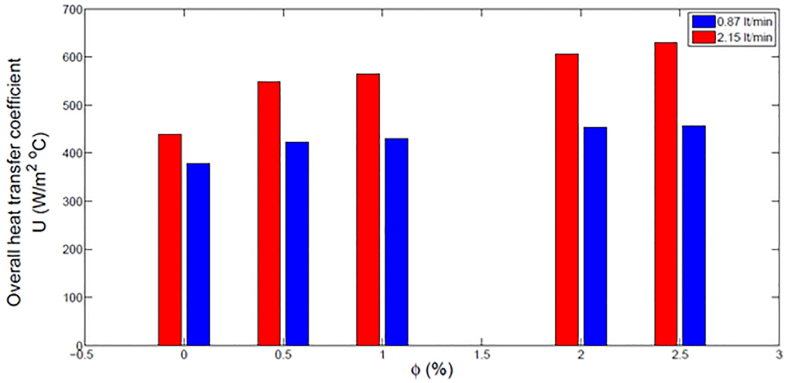

FIG. 6: Overall heat transfer coefficient versus solid particle volume fraction for two different values of inner pipe fluid volumetric flow rate, $T = 40°C$

difference for the overall heat transfer coefficient between the nanofluid (at the highest solid particle volume fraction) and the base fluid is 20.60%, whereas its value becomes 43.50% when the flow rate is increased to 2.15 L/min.

As compared to the numerical study, 12% and 19% higher values are obtained with water at volumetric flow rates of 0.87 L/min and 2.15 L/min. In the numerical study, 16% enhancement in the overall heat transfer coefficient is obtained for all flow rates, whereas this value deviates by about 4.6% and 27.5% at flow rates of 0.87 L/min and 2.15 L/min. The deviation between the experimental and numerical studies at the highest flow rate becomes higher.

Figure 7 demonstrates the effect of the inlet temperature of hot water entering the inner pipe for various solid particle volume fractions on the overall heat transfer coefficient. There is some slight enhancement in the heat transfer coefficient when the water temperature is increased for all solid particle volume fractions. This value is 2.78% for pure water and 2.49% for nanofluid with the highest particle volume fraction. This result supports the numerical one as the difference between the two temperatures becomes less than 2% for all solid particle volume fractions.

5. CONCLUSIONS

In this work, effects of inclusion of SiO_2 nanoparticles in a double-pipe heat exchanger performance were numerically and experimentally examined. The overall heat transfer coefficient was found to enhance with the inclusion of nanoparticles. In the numerical study, the rate of enhancement was found by about 16% whereas in the experimental study 20.60% and 43.50% enhancements are achieved for lowest and highest mass flow rates. There was very little

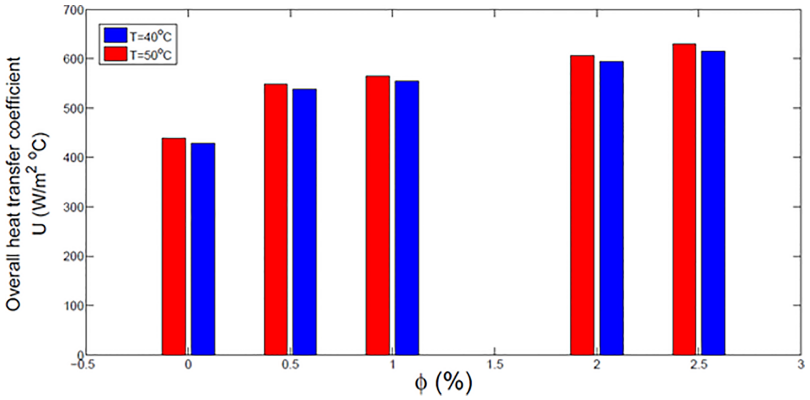

FIG. 7: Overall heat transfer coefficient versus solid particle volume fraction for two different values of inner pipe fluid temperature, $\dot{m} = 2.15$ L/min

influence of the inlet temperature on the heat transfer coefficient enhancement both in the numerical and in the experimental study.

REFERENCES

Aidaoui, L., Lasbet, Y., and Selimefendigil, F., Improvement of Transfer Phenomena Rates in Open Chaotic Flow of Nanofluid under the Effect of Magnetic Field: Application of a Combined Method, *Int. J. Mech. Sci*., vol. **179**, Article ID 105649, 2020.

Bahiraei, M., Rahmani, R., Yaghoobi, A., Khodabandeh, E., Mashayekhi, R., and Amani, M., Recent Research Contributions Concerning Use of Nanofluids in Heat Exchangers: A Critical Review, *Appl. Therm. Eng.*, vol. **133**, pp. 137–159, 2018.

Chen, M., He, Y., Huang, J., and Zhu, J., Investigation into Au Nanofluids for Solar Photothermal Conversion, *Int. J. Heat Mass Transf*., vol. **108**, pp. 1894–1900, 2017.

Chun, B., Kang, H.U., and Kim, S.H., Effect of Alumina Nanoparticles in The Fluid on Heat Transfer in Double-Pipe Heat Exchanger System, *Korean J. Chem. Eng*., vol. **25**, pp. 966–971, 2009.

Corcione, M., Heat Transfer Features of Buoyancy-Driven Nanofluids Inside Rectangular Enclosures Differentially Heated at the Sidewalls, *Int. J. Therm. Sci*., vol. **49**, pp. 1536–1546, 2010.

Demir, H., Dalkilic, A.S., Kürekci, N.A., Duangthongsuk, W., and Wongwises, S., Numerical Investigation on the Single Phase Forced Convection Heat Transfer Characteristics of TiO_2 Nanofluids in a Double-Tube Counter Flow Heat Exchanger, *Int. Commun. Heat Mass Transf*., vol. **38**, pp. 218–228, 2011.

Gürbüz, E.Y., Sözen, A., Variyenli, H.İ., Khanlari, A., and Tuncer, A.D., A Comparative Study on Utilizing Hybrid Type Nanofluid in Plate Heat Exchangers with Different Plates' Number, *J. Braz. Soc. Mech. Sci. Eng.*, vol. **42**, p. 527, 2020.

Ho, C.J., Guo, Y.-W., Yang, T.-F., Rashidi S., and Yan, W.-M., Numerical Study on Forced Convection of Water-Based Suspensions of Nanoencapsulated PCM Particles/Al_2O_3 Nanoparticles in a Mini-Channel Heat Sink, *Int. J. Heat Mass Transf.*, vol. **187**, Article ID 119965, 2020.

Kakaç, S., Liu, H., and Pramaunjaroenkij, A., *Heat Exchangers: Selection, Rating and Thermal Design*, Boca Raton, FL: CRC Press, 2020.

Khanlari, A., Sözen, A., Sahin, B., Di Nicola, G., and Afshari, F., Experimental Investigation on Using Building Shower Drain Water as a Heat Source for Heat Pump Systems, *Energy Sources, Part A: Recovery, Util. Environ. Effects*, pp. 1–13, 2020. DOI: 10.1080/15567036.2020.1796845

Khanlari, A., The Effect of Utilizing Al_2O_3–SiO_2/Deionized Water Hybrid Nanofluid in a Tube-Type Heat Exchanger, *Heat Transf. Res*., vol. **51**, no. 11, pp. 991–1005, 2020.

Mahbubul, I.M., Fadhilah, S.A., Saidur, R., Leong, K.Y., and Amalina, M.A., Thermophysical Properties and Heat Transfer Performance of Al_2O_3/R-134a Nanorefrigerants, *Int. J. Heat Mass Transf*., vol. **57**, pp. 100–108, 2013.

Maxwell, J.A., *Treatise on Electricity and Magnetism*, Oxford, UK: Oxford University Press, 1904.

Moravej, M., Bozorg, M.V., Guan, Y., Li, L.K.B., Doranehgard, M.H., Hong, K., and Xiong, Q., Enhancing the Efficiency of a Symmetric Flat-Plate Solar Collector via the Use of Rutile TiO_2–Water Nanofluids, *Sustain. Energy Technol. Assess.*, vol. **40**, Article ID 100783, 2020.

Saffarian, M.R., Moravej, M., and Doranehgard, M.H., Heat Transfer Enhancement in a Flat Plate Solar Collector with Different Flow Path Shapes Using Nanofluid, *Renew. Energy*, vol. **146**, pp. 2316–2329, 2020.

Selimefendigil, F. and Öztop, H.F., Corrugated Conductive Partition Effects on MHD Free Convection of CNT–Water Nanofluid in a Cavity, *Int. J. Heat Mass Transf.*, vol. **129**, pp. 265–277, 2019.

Selimefendigil, F. and Öztop, H.F., Effects of Nanoparticle Shape on Slot-Jet Impingement Cooling of a Corrugated Surface with Nanofluids, *J. Therm. Sci. Eng. Appl*., vol. **9**, Article ID 021016, 2017.

Selimefendigil, F. and Öztop, H.F., Performance Assessment of a Thermoelectric Module by Using Rotating Circular Cylinders and Nanofluids in the Channel Flow for Renewable Energy Applications, *J. Clean. Prod*., vol. **279**, Article ID 123426, 2021.

Shirvan, K.M., Mamourian, M., Mirzakhanlari, S., and Ellahi, R., Numerical Investigation of Heat Exchanger Effectiveness in a Double Pipe Heat Exchanger Filled with Nanofluid: A Sensitivity Analysis by Response Surface Methodology, *Powder Technol*., vol. **313**, pp. 99–111, 2017.

Sözen, A., Şirin, C., Khanlari, A., Tuncer, A.D., and Gürbüz, E.Y., Thermal Performance Enhancement of Tube-Type Alternative Indirect Solar Dryer with Iron Mesh Modification, *Sol. Energy*, vol. **207**, pp. 1269–1281, 2020.

Tuncer, A.D., Sözen, A., Khanlari, A., Gürbüz, E.Y., and Variyenli, H.İ., Analysis of Thermal Performance of an Improved Shell and Helically Coiled Heat Exchanger, *Appl. Therm. Eng*., vol. **184**, Article ID 116272, 2021.

Vajjha, R.S., Das, D.K., and Kulkarni, D.P., Development of New Correlations for Convective Heat Transfer and Friction Factor in Turbulent Regime for Nanofluids, *Int. J. Heat Mass Transf*., vol. **53**, pp. 4607–4618, 2010.

Vanaki, S.M., Mohammed, H.A., Abdollahi, A., and Wahid, M.A., Effect of Nanoparticle Shapes on the Heat Transfer Enhancement in a Wavy Channel with Different Phase Shifts, *J. Mol. Liq.*, vol. **196**, pp. 32–42, 2014.